ELSEVIER

Fusion Engineering and Design 36 (1997) 479–503

Fusion Engineering and Design

Kerma factor evaluation and its application in nuclear heating experiment analysis

Li Zhang *, M.A. Abdou

University of California at Los Angeles, Los Angeles, CA 90095, USA

Received 15 January 1996; accepted 20 October 1996

Abstract

The accuracy of calculating 'kerma factor', which is the response function for nuclear heating is very important in many applications, particularly fusion systems. A computer code, called MAZE, has been developed primarily for evaluating neutron and gamma kerma factors based on an improved modeling and a capability to analyze basic data and evaluate consistency in preserving energy. Kinematics equations and energy conservation considerations are modeled in the code. The code has features that allow comparison and analysis among different methods of calculating the kerma factor and it provides users with data information needed to make user-oriented selections from two to three, often different, results. A kerma factor library, called MAZE-LIB, has been generated with MAZE for most of the materials of interest in fusion based on the most recent and accurate data available, FENDL library, which is the nuclear data library selected by ITER. The kerma factor library provided in this work is the result of an extensive analysis of nuclear data and careful selection from among often different results from the different calculational methods. It was shown that some data inconsistency problems in preserving the energy still exist in the FENDL library. Some problems with the widely used computer code NJOY were exposed during the process of the kerma factor evaluation, which is crucial at this stage of fusion research, since NJOY is the primary nuclear data processing code selected by ITER. Comparison with nuclear heating experimental data, derived from very recent integral experiments with 14 MeV neutrons and the analysis of the uncertainty in prediction have been carried out using the newly developed kerma factors. Comparative analysis shows that the new kerma factors generated in this work result in better agreement with the experiments than those obtained from previous work. The calculated-to-experimental values (C/Es) obtained in this work indicate an overestimation of the gamma production in the basic nuclear data library for certain elements. The integral and differential heating profiles along with knowledge of the contributing partial kerma factors, which are generated in this work, could in principle, provide input for sensitivity analysis and be used to improve the basic nuclear data and kerma factor evaluations. © 1997 Elsevier Science S.A.

Keywords: Kerma factor; MAZE; NJOY

* Corresponding author. Environmental Control Systems, Douglas Aircraft Company, Internal Mail Code D800-0034, 3855 Lakewood Blvd., Long Beach CA 90846, USA. Tel.: +1 310 4975341; fax: +1 310 5937352.

PII S0920-3796(96)00704-1

1. Introduction

In any nuclear systems, accurate calculation of nuclear heating is necessary for the prediction and analysis of the thermomechanical performance, safety, radiation protection of components and biological dose. The nuclear heating is the sum of neutron heating and gamma heating. The neutron heating is the local energy deposition by the recoil nucleus and charged particles emitted from neutron interactions with matter. Gamma heating is the local energy deposition from gamma-ray interactions, the most important of which are photoelectric, pair production and Compton scattering. Normally, gamma heating calculations are simple because gamma-ray interactions are well understood and the reaction cross sections are known accurately and can be expressed analytically. In general, the major source of inaccuracy in the calculation of gamma heating is errors in calculating the gamma-ray production source. In contrast, neutron heating calculations can be complex because of the enormous amount of basic nuclear data required. In a fusion system operated on the Deuterium–Tritium fuel cycle, the neutron spectrum extends from very low energies to about 15 MeV. The variety of possible neutron induced reactions and the multiplicity of reaction products make neutron heating calculations relatively difficult. The difficulty is compounded by the lack of some data or inaccuracies in available ones.

The key response function for neutron heating is the neutron kerma factor. Abdou [1] used momentum and energy conservation principles to derive expressions for calculation of neutron kerma factors. He also developed a code to process and analyze basic nuclear data and to calculate kerma factors from available data libraries. In his code, he also used energy conservation to check and correct for inconsistencies in basic nuclear data. Other authors, e.g. Farawila [2], introduced further improvements in order to utilize newly available nuclear data in kerma factor calculations.

In the present work, we report on the following:

- extending Abdou's model to make use of new basic data that has become available in the past several years and to introduce additional algorithms for checking and correcting inconsistencies in available data;
- the development of a new code, MAZE, which allows processing of newly available nuclear data libraries in the most recent format, called ENDF/B-VI;
- the generation of a new kerma factor library, called MAZE-LIB, for most materials of interest in fusion and other applications based on the most recent and accurate data available; and
- comparison of nuclear heating predictions from the newly generated library with the results of integral experiments recently conducted in a joint collaboration between Japan and USA.

Section 2 is a review of Abdou's model and the improvements introduced in the present work. Section 3 highlights the MAZE code development. Sections 4–7 summarize the data processing and the generation of the new library. Section 8 compares the kerma factors generated in this work to those obtained from an existing code. Section 9 compares the calculational results obtained using the results of the present work to those measured in recent integral experiments. The source of discrepancies between the calculated and measured values are also discussed. Section 10 discusses the importance of gamma heating in fusion reactor system. The final section summarizes the conclusions.

2. Evaluation model review and improvements

The nuclear heating at a spatial point $\boldsymbol{r}$ is the sum of neutron heating and gamma heating, and each can be expressed as [1]:

$$\begin{aligned} H_{\mathrm{n}}(\boldsymbol{r}) &= \sum_j N_j(\boldsymbol{r}) \int \Phi_{\mathrm{n}}(\boldsymbol{r}, E_{\mathrm{n}}) \sum_i \sigma_{\mathrm{n}ij}(E_{\mathrm{n}}) h_{\mathrm{n}ij}(E_n)\, \mathrm{d}E_{\mathrm{n}} \\ &= \sum_j N_j(\boldsymbol{r}) \int \Phi_{\mathrm{n}}(\boldsymbol{r}, E_{\mathrm{n}}) \sum_i k_{\mathrm{n}ij}(E_{\mathrm{n}})\, \mathrm{d}E_{\mathrm{n}} \\ &= \sum_j N_j(r) \int \Phi_{\mathrm{n}}(\boldsymbol{r}, E_{\mathrm{n}}) K_{\mathrm{n}j}(E_{\mathrm{n}})\, \mathrm{d}E_{\mathrm{n}} \end{aligned} \tag{1}$$

$$H_\gamma(\boldsymbol{r}) = \sum_j N_j(\boldsymbol{r}) \int \Phi_\gamma(\boldsymbol{r}, E_\gamma) \sum_i \sigma_{\gamma ij}(E_\gamma) h_{\gamma ij}(E_\gamma)\, \mathrm{d}E_\gamma$$
$$= \sum_j N_j(\boldsymbol{r}) \int \Phi_\gamma(\boldsymbol{r}, E_\gamma) \sum_i k_{\gamma ij}(E_\gamma)\, \mathrm{d}E_\gamma$$
$$= \sum_j N_j(\boldsymbol{r}) \int \Phi_\gamma(\boldsymbol{r}, E_\gamma) K_{\gamma j}(E_\gamma)\, \mathrm{d}E_\gamma \qquad (2)$$

where: $H_n(\boldsymbol{r})$ = neutron heating rate at position $\boldsymbol{r}$ (eV cm^{-3} s^{-1}); $H_\gamma(\boldsymbol{r})$ = gamma heating rate at position $\boldsymbol{r}$ (eV cm^{-3} s^{-1}); $\Phi_n(\boldsymbol{r}, E_n)$ = neutron flux at position $\boldsymbol{r}$ and energy E_n (neutrons cm^{-2} eV^{-1} s^{-1}); $\Phi_\gamma(\boldsymbol{r}, E_\gamma)$ = gamma flux at position $\boldsymbol{r}$ and energy E_γ (gamma cm^{-2} eV^{-1} s^{-1}); $N_j(\boldsymbol{r})$ = number density of element j at position $\boldsymbol{r}$ (atom cm^{-3}); $\sigma_{nij}(E_n)$ = microscopic neutron cross section of element j for reaction i at energy E_n(cm^2 atom^{-1}); $\sigma_{\gamma ij}(E_\gamma)$ = microscopic gamma cross section of element j for reaction i at energy E_γ (cm^2 atom^{-1}); h_{nij} = energy deposited per neutron reaction i in element j (eV); $h_{\gamma ij}$ = energy deposited per gamma reaction i in element j (eV); $k_{nij}(E_n) = \sigma_{nij}(E_n)h_{nij}(E_n)$, partial neutron kerma factor for reaction i element j at energy E_n (eV cm^{-2} atom^{-1}); $k_{\gamma ij}(E_\gamma) = \sigma_{\gamma ij}(E_\gamma)h_{\gamma ij}(E_\gamma)$, partial gamma kerma factor for reaction i element j at energy E_γ (eV cm^{-2} atom^{-1}); $K_{nj}(E_n) = \Sigma_i k_{nij}(E_n)$, microscopic neutron kerma factor for element j at energy E_n (eV cm^{-2} atom^{-1}); $K_{nj}(E_n) = \Sigma_i k_{\gamma ij}(E_\gamma)$, microscopic gamma kerma factor for element j at energy E_γ (eV cm^{-2} atom^{-1}) = $\sigma^j_{pe}(E_\gamma)E_\gamma + \sigma^j_{pp}(E_\gamma - 1.02e+6) + \sigma^j_{cs}(E_\gamma)(E_\gamma - E'_\gamma)$; $\sigma^j_{pe}(E_\gamma)$ = photoelectric microscopic cross section for element j (cm^2); $\sigma^j_{pp}(E_\gamma)$ = pair production microscopic cross section for element j (cm^2); $\sigma^j_{cs}(E_\gamma)$ = Compton scattering microscopic cross section for element j (cm^2); E'_γ = energy of scattered photon (eV).

Here it is assumed that photoelectric, pair production and Compton scattering are the only contributing processes to the gamma heating.

Since the mechanisms of gamma interactions with materials are well understood, determination of the gamma kerma factors presents no problem. However, information about gamma production is not always given in satisfactory detail or accuracy. This affects the calculations of gamma heating as well as that of neutron heating. In addition, the calculation of neutron kerma factors is complicated due to the emission of more than one particle in many reactions. There are large uncertainties in the data and calculation of neutron kerma factors.

The physics behind neutron heating is conservation of energy and conservation of linear momentum. However, even for the simplest reaction, namely elastic scattering, an accurate calculation of the kerma factors depends on the spectrum of the secondary neutron, which in turn depends on the nuclear data obtained from experiments and calculations based on nuclear models. As indicated in early work by Abdou and Maynard [1], "the limitation on the accuracy of a neutron kerma calculation is determined by the availability and accuracy of the nuclear data" and that in turn, is determined by experiments and data evaluation. For reader's convenience, the neutron kerma factor evaluation models from the previous works [1] and [2] are summarized here. The gamma kerma factor evaluation model is also discussed with the focus on Compton scattering reaction.

2.1. Neutron kerma factor evaluation model

2.1.1. Kinematics: energy and linear momentum conservation

Reaction kinematics utilizes two basic laws of physics: energy and linear momentum conservation. These two laws are all the physics needed to calculate kerma factors. Therefore, it can be said that kinematics is the only method used to calculate kerma factors.

However, there are different ways of applying kinematics to the nuclear data library, depending upon the type of data available. There are cases where only the energy conservation law can be used because there is not enough data to solve the momentum equations (e.g. lack of energy and angular distribution data for secondary particles), this approach is often referred to as the energy balance method. In other cases where both conservation laws can be applied to derive kerma factors from the data library (e.g. elastic scattering). There are also cases where one can apply

either one of the methods mentioned above. Unfortunately, from past experiences, different approaches often lead to different results, exposing inconsistencies in the data. They are all part of kinematics but they use different parts of the data library. That is why they are sometimes referred to as the direct energy balance and the kinematics method (whenever liner momentum conservation is applied). For the sake of convenience, the two approaches will still be referred to in this study as the kinematics method and the balance method given one understands the meaning behind them. A third approach becomes possible with the availability of the ENDF/B-VI [3] format libraries where, in file 6, energy and angular distributions are given for all the products of nuclear reactions. Kerma factors can then be derived from the data of the recoil nucleus and the charged particles alone through:

$$k_{ni}(E_n) = \sigma_i(\bar{E}_{rec} + \bar{E}_x) \tag{3}$$

where $\bar{E}_{rec}$ and $\bar{E}_x$ denote the average energy of recoil target and the average energy of charged particles, respectively. The results from the three approaches are referred to, in this study, as the balance result, the kinematics result and the recoil result.

The reason for the discrepancy among the different results is that the nuclear data libraries, such as ENDF/B, were developed primarily for neutron and gamma transport and local conservation of energy was not always a major concern. When scientists tried to make use of the data libraries by applying the energy balance scheme to come up with kerma factors, they found missing data and negative kermas, which is why they went back and employed the full kinematics equations. Given the status of nuclear libraries, the kinematics relations for various reactions should be employed when possible to serve as a tool to check upon data consistency, even if energy conservation alone is sufficient to derive kerma factors from the data libraries.

2.1.2. Energy balance (or energy conservation)

The prompt neutron microscopic kerma factor K (no decay energy is considered here) for a given element at incident energy E can be expressed as:

$$K = \sum_i \sigma_i h_i = \sum_i \sigma_i (E_n + Q_i - \bar{E}_{n'i} - \bar{E}_{\gamma i}) \tag{4}$$

which is a basic energy balance equation. The overline means average over all secondary particles and their energy. However, the information for gamma production is not always given for each individual reaction in the library. Instead, gamma production data are usually lumped together for several reactions, e.g. non-elastic plus radiative capture gammas. In this case, Eq. (4) has to be rearranged:

$$K = \sum_i \sigma_i (E_n + Q_i - \bar{E}_{n'i}) - \sum_j \sigma_{\gamma j} \bar{E}_{\gamma j} \tag{5}$$

Due to the nature of the (n, γ) data in ENDF/B, the kerma factor for radiative capture needs to be singled out. According to ENDF/B rules, $\bar{E}_\gamma$ in the (n, γ) reaction follows:

$$\bar{E}_\gamma = Q + E_n \frac{A}{A+1} \tag{6}$$

therefore,

$$h_{(n,\gamma)} = E_n + Q - \bar{E}_\gamma = E_n \frac{1}{A+1} \tag{7}$$

where A is the ratio of target nucleus mass to the neutron mass. But according to kinematics,

$$h_{(n,\gamma)} = \frac{E_n}{A+1} + \frac{1}{2(A+1)m_n c^2} \bar{E}_\gamma^2 \tag{8}$$

where $m_n c^2$ is the neutron rest mass energy. The second term in Eq. (8) represents only 0.1% of the total photon energy, and thus it does not affect the accuracy of $\bar{E}_\gamma$. However, it can sometimes dominate the total kerma when the incident neutron is of low energy. So Eq. (5) has to be rearranged as:

$$K = \sum_{i, i \neq (n,\gamma)} \sigma_i (E_n + Q_i - \bar{E}_{ni}) - \sum_{j, j \neq (n,\gamma)} \sigma_{\gamma j} \bar{E}_{\gamma j} + K_{n,\gamma} \tag{9}$$

where Eq. (8) is used for (n, γ) kerma factor calculation. Eq. (9) is the basic form of energy balance when applying it to a nuclear data library. The major disadvantage of this is its precision problem. Consider

$$h_i = E_n + Q_i - \bar{E}_{n'i} - \bar{E}_{\gamma i} \tag{10}$$

The magnitude of h_i is usually much smaller than that of the individual terms on the right hand side of Eq. (10), thus the required precision of the secondary neutron and gamma energy can sometimes be impractical. If inaccuracies occur in the data library, Eq. (10) will lead to inaccurate results.

2.1.3. Kinematics relations for important nuclear reactions

Nuclear reactions are classified in the ENDF/B library by the MT numbers. Since local energy deposition is caused by the recoil nucleus and charged particle (decay energy is not considered at this moment), kinematics is used to calculate the recoil energy for each reaction [4]. However, when information about the energy distribution of the secondary particles are missing the kinematics method can not be applied.

Elastic scattering (MT = 2)

$$n + A \rightarrow n' + A \quad (Q = 0)$$

By applying kinematics, the recoil energy of the target ($\bar{E}_r$) and the energy of the scattered neutron ($\bar{E}_n$) are found to have the following forms:

$$h = \bar{E}_r = \frac{2AE_n}{(A+1)^2}(1 - \mu_{cm}) \tag{11}$$

$$\bar{E}_{n'} = E_n - \bar{E}_r = \frac{A^2 + 2A\bar{\mu}_{cm} + 1}{(A+1)^2} E_n \tag{12}$$

where A is the ratio of target nucleus mass to neutron mass. The average cosine of the secondary neutron scattering angle in the center of mass system, $\bar{\mu}_{cm}$ is obtained from the angular distribution data in ENDF/B file 4.

Inelastic scattering to level (MT = 51–90)

$$n + A \rightarrow n' + A^*$$

where A^* means the target nucleus is left at an excited energy level, E^*_λ. Kinematics leads to the following equations:

$$\bar{E}_r = \frac{2AE_n}{(A+1)^2}\left(1 - \bar{\mu}_{cm}\sqrt{1 - (A+1)E^*_\lambda/(AE_n)}\right) - \frac{E^*_\lambda}{(A+1)} \tag{13}$$

$$\bar{E}_{n'} = E_n - \bar{E}_r \tag{14}$$

When de-excitation is carried out by photon emission, $h = \bar{E}_r$. De-excitation by charged particle emission results in $h = \bar{E}_r + E^*_\lambda + Q_C$, where Q_C is the mass deficit associated with the charged particle emission ($A^* \rightarrow B +$ particles, $Q_c = (M_A - M_B - M_p)c^2$).

Inelastic scattering to continuum (MT = 91)

$$n + A \rightarrow n' + A^*$$

The angular distribution data for the secondary neutron in the laboratory system is provided in ENDF/B file 4. The average recoil energy is calculated by kinematics:

$$\bar{E}_r = \frac{1}{A}(E_n + \bar{E}_{n'} - 2\bar{\mu}_L\sqrt{E_n}\langle\sqrt{E_{n'}}\rangle) \tag{15}$$

where $\bar{\mu}_L$ is the average cosine of the secondary neutron scattering angle in the laboratory system, and $\langle\sqrt{E_{n'}}\rangle$ is the average of the square root of the secondary neutron energy weighted by its energy spectrum given in ENDF/B file 5. If the value of $\mu_L = 0$ is found in file 4, a better assumption of isotropy in the center of mass system is made instead of using a zero value. The average recoil energy is in the form

$$\bar{E}_r = \frac{(A-1)E_n}{A(A+1)} + \frac{\bar{E}_{n'}}{A} \tag{16}$$

Eqs. (15) and (16) are applicable only for gamma emission of de-excitation. For charged particle emission, other equations apply.

Radiative capture (MT = 102)

$$n + A \rightarrow (A+1) + \gamma$$

Eq. (8) is used to calculate capture reaction when capture gamma files are given in ENDF/B data. If that information is missing, the following equation derived from kinematics can be used instead:

$$\bar{E}_r = E_n + Q + (A+1) \times m_n c^2\left(1 - \sqrt{1 + \frac{2}{(A+1)m_n c^2}\left(Q + \frac{AE_n}{A+1}\right)}\right) \tag{17}$$

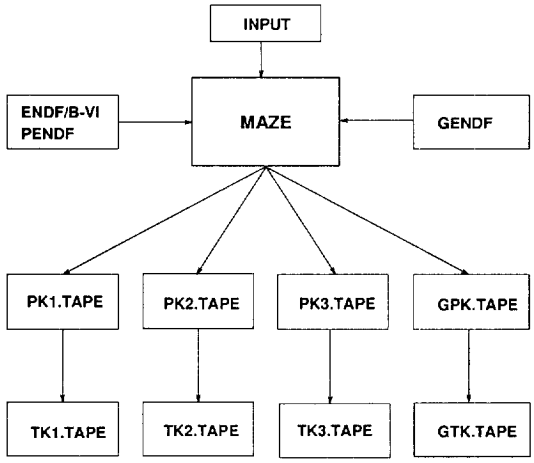

Fig. 1. MAZE input and output.

Direct (n, 2n) reaction (MT = 16)

$$n + A \rightarrow (A-1)^* + 2n'$$

By solving the kinematics equations one can get:

$$\bar{E}_r = \frac{1}{(A-1)}[E_n + E_{n_1} + E_{n_2} - 2\mu_1\sqrt{E_n E_{n_1}} - 2\mu_2\sqrt{E_n E_{n_2}} + 2\mu_1\mu_2\sqrt{E_{n_1} E_{n_2}} + 2\sqrt{E_{n_1} E_{n_2}}\sqrt{(1-\mu_1^2)(1-\mu_2^2)}\cos(\phi_1 - \phi_2)] \quad (18)$$

Where E_{n_1}, and E_{n_2} are the two secondary neutron energies, μ_1 and μ_2 are the cosines of the scattering angles in the laboratory system, and ϕ_1 and ϕ_2 are the azimuthal angles. In the ENDF/B file

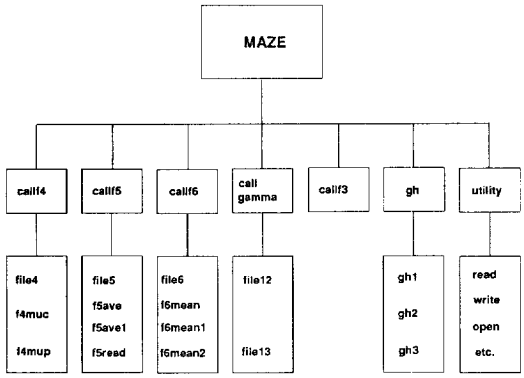

Fig. 2. MAZE program layout.

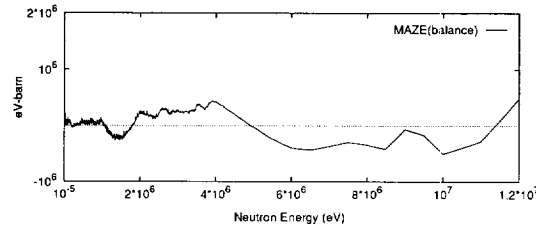

Fig. 3. Total prompt neutron kerma factor of Ti.

no azimuthal information is available, instead, $\cos(\phi_1 - \phi_2)$ is assumed to be zero. Since the two neutrons are indistinguishable in the ENDF/B data, the following assumptions have to be made:

$$E_{n'} = (E_{n_1} + E_{n_2})/2 \quad (19)$$

$$\sqrt{E_{n'}} = (\sqrt{E_{n_1}} + \sqrt{E_{n_2}})/2 \quad (20)$$

$$\langle \mu_1\mu_2 \rangle = \bar{\mu}_L^2 \quad (21)$$

$$\langle \sqrt{E_{n_1} E_{n_2}} \rangle = \bar{E}_{n'} \quad (22)$$

Eq. (18) then becomes:

$$\bar{E}_r = \frac{1}{A-1}(E_n + 2\bar{E}_{n'}(1+\bar{\mu}_L^2) - 4\bar{\mu}_L\sqrt{E_n \bar{E}_{n'}}) \quad (23)$$

Isotropic (n, mn) reactions

$$n + A \rightarrow (A - m + 1)^* + mn$$

The energy of m neutrons can be found in ENDF/B file ($m = 2$, 3, or 4) without distinguishing individual neutrons. With the center-of-mass isotropy assumption, the average recoil energy can be obtained from:

$$\bar{E}_r = \frac{(A-m)(A+2-m)}{(A+1)^2(A+1-m)} E_n + \frac{\bar{E}_{mn}}{(A+1-m)} \quad (24)$$

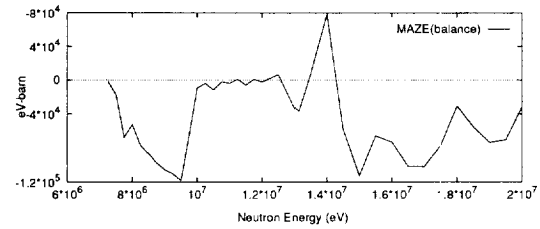

Fig. 4. Partial neutron kerma factor of W186 (n, 2n).

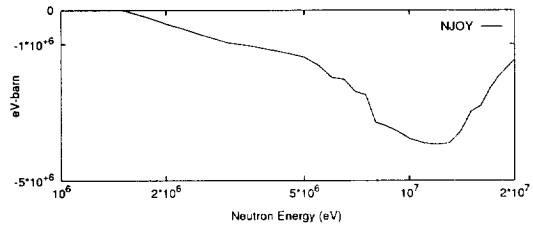

Fig. 5. Partial neutron kerma factor of Si (n, n'), NJOY.

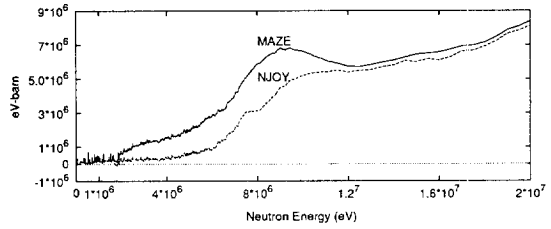

Fig. 7. Total prompt neutron kerma factor of Si.

(n, mn) Charged particle (m = 0, 1, 2)

Detailed information about the energy distribution of charged particles are scarce in the ENDF/B data, thus requiring the energy balance methods to be used:

$$h = \bar{E}_r + \bar{E}_x = E_n + Q_0 - \bar{E}_{mn} - E^* \tag{25}$$

where E^* is the residual excitation energy, $\bar{E}_{mn}$ is the average energy of all m secondary neutrons, and $\bar{E}_x$ is the average energy of the charged particle.

2.1.4. Energy release from fission

By using the energy-dependent yields of fission products, the energy-dependent Q-value can be calculated from:

$$Q(E_n) = c^2\left[M - \sum_j Y_j(E_n)M_j - (\bar{\nu}(E_n) - 1)m_n\right] \tag{26}$$

where $Y_j(E_n)$ is the yield of the fission product j, M_j is the mass of the fission product j, M is the fissionable nucleus mass, m_n is the rest mass of the neutron, and $\bar{\nu}(E_n)$ is the average number of fission neutrons.

The local energy deposition can be obtained from the energy balance as:

$$h = E_n + Q(E_n) - E_{n'} - E_\gamma - E_\nu \tag{27}$$

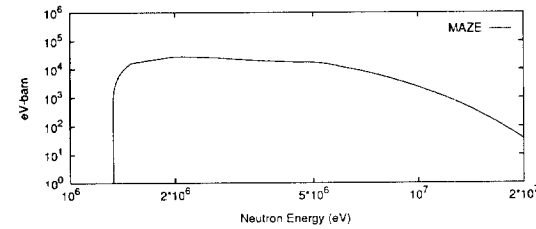

Fig. 6. Partial neutron kerma factor of Si (n, n'), MAZE.

where E_ν is the unrecoverable energy carried away by neutrinos and antineutrinos, $E_{n'}$ and E_γ are the total energy carried away by neutrons and gamma rays respectively.

2.1.5. Natural elements

The equations described so far can only be applied to materials with a single isotope. In the case of natural elements with more than one isotope, some modifications have to be made. The Q value is no longer energy independent, the definition of $Q_m(E)$ for the mixture follows:

$$Q_m(E_n) = \frac{\Sigma_j \sigma_j(E_n)N_j Q_j}{\Sigma_j \sigma_j(E_n)N_j} \tag{28}$$

where m denotes mixture and j denotes isotope. Similar definitions can be derived for other physical quantities, e.g. energy of secondary neutron, decay energy, etc.

It can be seen from the above equation that a property that is energy independent for an isotope becomes energy dependent for a mixture if it is weighted by cross sections. Also, if nuclear data is available only for the mixture but not for each isotope, then the kerma factor cannot be accurately calculated.

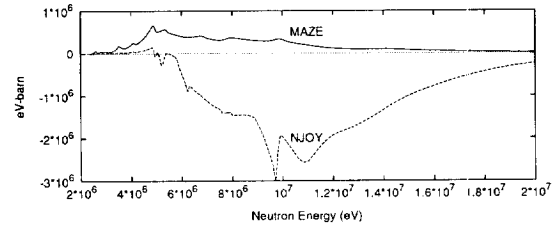

Fig. 8. Partial neutron kerma factor of B11 (n, n').

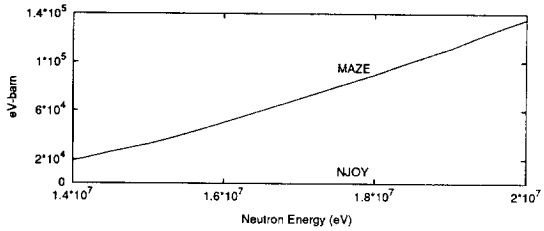

Fig. 9. Partial neutron kerma factor of B11 (n, 2n).

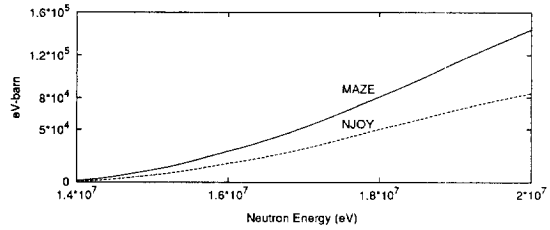

Fig. 11. Partial neutron kerma factor of B11 (n, np).

2.1.6. Energy deposition due to radioactive decay

The decay energy of the activated residual nuclei is time dependent. However, if the contribution of radioactive decay is not significant compared to the total heating and if a cutoff time is used to neglect the activated isotopes that have a half life more than the cutoff time (e.g. 1 day), then the decay energy can be treated as time independent. For example, if nuclear reaction i induces β^- decay, then a partial kerma factor of decay caused by reaction i, k_{id}, can be obtained through:

$$k_{id} = \sigma_i \bar{E}_{\beta^-} \tag{29}$$

where σ_i is the cross section of the reaction i and $\bar{E}_{\beta^-}$ is the average energy of the β^- particle; k_{id} can then be added to the prompt kerma factor of reaction i. The decay energy of the charged particles and gamma rays should be treated separately because the charged particles deposit energy locally while gamma rays transport it somewhere else. Gamma yield from decay can be added to total gamma production cross sections.

β^- emission is the most frequent type of decay. The maximum energy can be obtained by a mass balance. The average energy can be calculated using an average-to-maximum ratio table produced by Abdou [1]. For detailed afterheat analysis, special codes have to be used.

2.2. Gamma kerma factor evaluation model

The three major contributing reactions for gamma kerma factors in the energy range of fusion systems are the photoelectric, Compton or incoherent scattering and pair production reactions (see Eq. (30)).

$$K_{\gamma j}(E_\gamma) = \sigma^j_{\mathrm{pe}}(E_\gamma)E_\gamma + \sigma^j_{\mathrm{pp}}(E_\gamma - 1.02) + \sigma^j_{\mathrm{cs}}(E_\gamma)(E_\gamma - E'_\gamma) \tag{30}$$

It is assumed that all the gamma energy in the photoelectric reaction is deposited locally and all the gamma energy in pair production reaction minus 1.02 MeV (energy of electronpositron mass) is deposited locally. In the incoherent scattering reaction, the photon only deposits a fraction of its energy to the local media and the scattered photon carries the rest away. The calculation of the deposited energy is not easily done. The equations used in MAZE for calculation of the average energy of scattered gamma rays from incoherent scattering are [5]:

$$\sigma_I(E_\gamma, E'_\gamma, \mu) = S(q, Z)\sigma_{\mathrm{KN}}(E_\gamma, E'_\gamma, \mu) \tag{31}$$

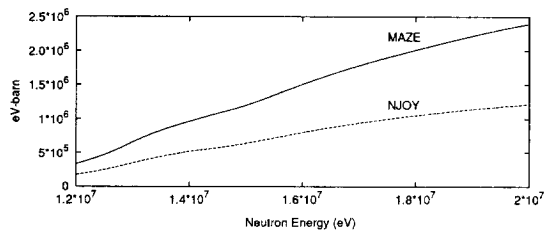

Fig. 10. Partial neutron kerma factor of B11 (n, nα).

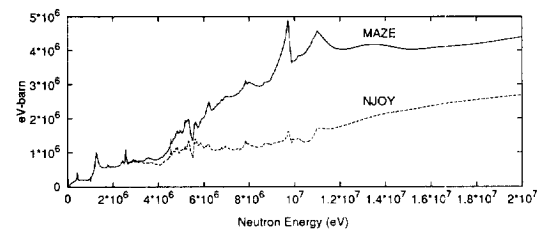

Fig. 12. Total prompt neutron kerma factor of B11.

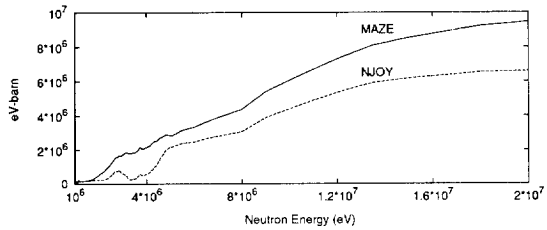

Fig. 13. Total prompt neutron kerma factor of P.

$$\sigma_{KN}(E_\gamma, E'_\gamma, \mu) = \frac{3\sigma_T k'^2}{8k^2}\left[\frac{k}{k'} + \frac{k'}{k} + 2(\mu - 1) + (\mu - 1)^2\right] \quad (32)$$

$$k = \frac{E_\gamma}{m_e c^2}$$

$$k' = \frac{E'_\gamma}{m_e c^2}$$

$$\sigma_T = 0.6652448 \ barn$$

$$\mu = 1 + \frac{1}{k} - \frac{1}{k'} \quad (33)$$

$$q = 2k\sqrt{0.5(1-\mu)}\,\frac{1 + 0.5(k^2 + 2k)(1-\mu)}{1 + k(1-\mu)} \quad (34)$$

from Eqs. (33) and (34):

$$k' = k + 1.0 - \sqrt{1.0 + q^2} \quad (35)$$

where: σ_I = incoherent scattering cross section (barn); σ_{KN} = Klein-Nishina collision cross section per electron (barn); σ_T = Thomson scattering cross section (barn); $S(q, z)$ = incoherent scattering function; q = momentum transfer to an atom, in units of electron mass; k = gamma energy in units of electron mass; k = scattered gamma energy in units of electron mass.

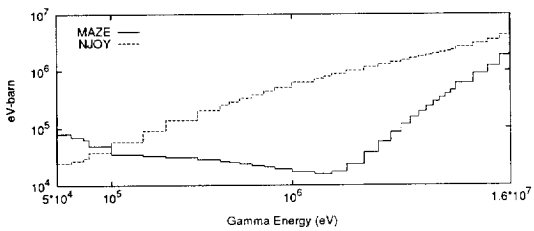

Fig. 14. Total gamma kerma factor of C, MAZE and MATXS15.

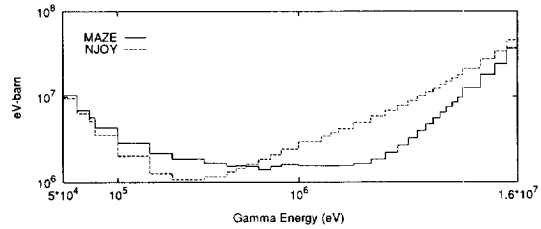

Fig. 15. Total gamma kerma factor of Ni, MAZE and MATXS15.

$S(q, Z)$ is tabulated in ENDF/B-VI where q is in units of inverse angstroms. To convert q from units of inverse Å to units of electron mass, a conversion factor of 0.048526 is used.

3. Code development

Although NJOY[6] can process ENDF/B-VI formatted libraries and generate kerma factors, the code does not function as an evaluation tool since NJOY was developed primarily as a data processing code. To evaluate, select and compile the best kerma factor library, a new code with convenient features for comparative analysis is needed. The new code should be more of an evaluation tool rather than a mere data processing code. The new code can also be used to validate the NJOY results to ensure that the kerma factor calculation is done correctly, as is done with many radiation transport codes (ANISN [9], ONDENT [10], etc.). As will be seen later, the development of the new code did expose some problems with NJOY which is crucial at this stage of fusion research, since NJOY is the primary data processing code selected by ITER.

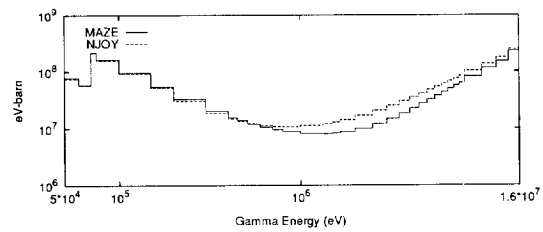

Fig. 16. Total gamma kerma factor of W, MAZE and MATXS15.

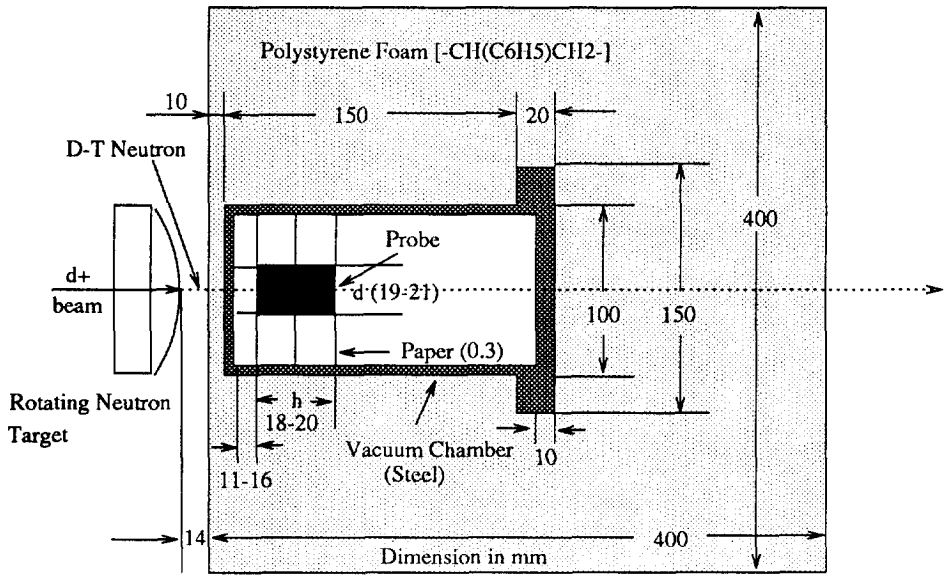

Fig. 17. USDOE/JAERI nuclear heating experiment configuration [11].

Other codes for kerma factor calculation, such as MACK-IV [7] and KAOS [8], were developed for the earlier versions of ENDF library and no longer process the new ENDF/B-VI formatted libraries.

To this end, a computer code, called MAZE, has been developed primarily for evaluating neutron and gamma kerma factors based on improved approach to data library and calculational algorithms. These improved algorithms are based on kinematics and energy conservation considerations. The code has features that allow comparison and analysis among the different methods of calculating the kerma factor and it provides users with data information needed to make application-oriented selections from the two to three often different results. MAZE can work with nuclear data libraries that are either in ENDF/B-V or ENDF/B-VI format. The code was organized in a highly modularized manner so that further modification and enhancement can be incorporated easily. The code organization also gives a clear picture of the data processing procedure as shown in Fig. 1 and Fig. 2.

The nuclear data files required by MAZE are:

ENDF/B-VI etc.	Neutron nuclear data of ENDF/B-VI or ENDF/B-V format
PENDF	Neutron nuclear data after resonance and broadening treatment by NJOY

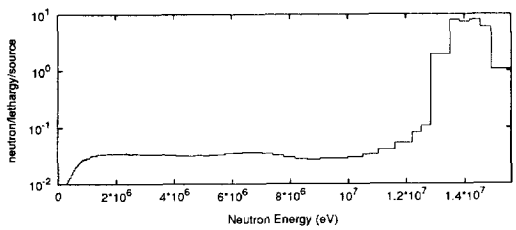

Fig. 18. Neutron source spectrum coming out of the target.

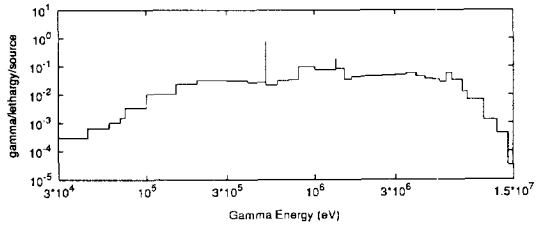

Fig. 19. Gamma source spectrum coming out of the target.

Table 1
Comparison Between the Calculated and the Experimental Results

Material	Specific heat (J g^{-1} K^{-1})	Measured value K source^{-1} s^{-1}	C/E			
			MAZE			MATXS15
			Bal[a]	Kin[b]	Rec[c]	
C	0.712	1.087–16	0.87			0.97
	0.527		1.15			1.28
Ti	0.527	3.769–17	0.97	1.03		0.45
Ni	0.444	7.443–17			0.99	1.19
Zr	0.284	6.291–17	0.70	0.73		1.07
W	0.133	9.405–17		1.36		1.69
Pb	0.128	8.681–17			1.28	1.59

[a] Balance kerma factor evaluation.
[b] Kinematics kerma factor evaluation.
[c] Recoil kerma factor evaluation.

GENDF Gamma nuclear data of ENDF/B-V or ENDF/B-VI format

The input file contains information regarding material number, library version (ENDF/BV or ENDF/B-VI), the negative partial kerma flag which indicates whether to keep them or to set them zeros, the decay flag indicates whether to include or not to include the decay energy and the reaction number and average decay energy if the decay flag is on.

The various output tapes have the following meaning:

pk1.tape Partial neutron kerma factor using kinematics relations
pk2.tape Partial neutron kerma factor using balance relations
pk3.tape Partial neutron kerma factor using the recoil and charged particle spectrum in file 6
gpk.tape Partial gamma kerma factor
tk[1-3].tape Corresponding total neutron kerma factor from pk[1-3].tape
gtk.tape Total gamma kerma factor

The output file has data information extracted from the library, e.g. laboratory system for secondary particles, interpolation schemes and the format of the data. It also has warning or error messages and data processing information to help the user to diagnose any problem, to analyze the data, and to make the selections of the kerma factors.

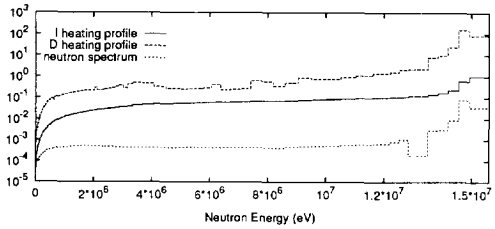

Fig. 20. Neutron profiles of C probe.

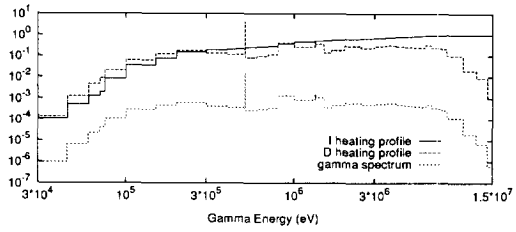

Fig. 21. Gamma profiles of C probe.

Table 2
Contributions from different energy ranges, C

Neutron (99%)		Gamma (1%)	
Energy range (MeV)	Contribution (%)	Energy range (MeV)	Contribution (%)
0.0–0.8	~1	0.0–0.15	~5
0.8–11.6	~9	0.15–10.0	~92
11.6–15.6	~90	10.0–14.0	~3

4. Data processing of nuclear data library in MAZE

The computer code MAZE consists of six major branches (Fig. 2) which handle different types of nuclear data:

Callf4	Processes file 4 data and generates neutron kerma factors for the elastic and inelastic reactions.
Callf5	Processes file 5 data to calculate the average energy of the secondary neutrons for reactions like (n, 2n), (n, np)
Callf6	Derives the spectrums of neutrons, gammas, charged particles and recoil nucleus. The neutron and gamma data are used to derive the balance result. The recoil target data and the charged particles data are used to derive the recoil result
Callgamma	Processes file 12 and file 13 data to get the average energy of the gamma rays from various nuclear reactions
Callf3	Handles reactions in file 3 that don't produce secondary neutrons, like (n, charged particle) reaction
gh	Generates the gamma kerma factors from file 23 and file 27
Utility	A subroutine package which carries out operations like opening, reading, writing, interpolation, integration and so on

For detailed information regarding MAZE, please refer to MAZE manual to be submitted to the Radiation Shielding Information Center.

5. Evaluation of kerma factor and generation of a reference library for commonly used materials

The nuclear data for a large number of materials were processed and evaluated. Kerma factors

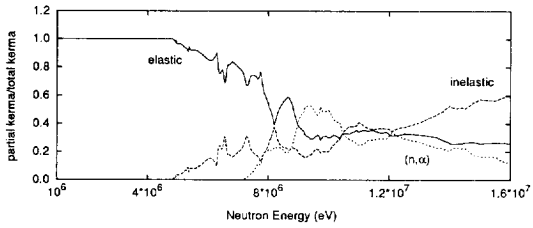

Fig. 22. Contributing neutron partial kerma factors, C.

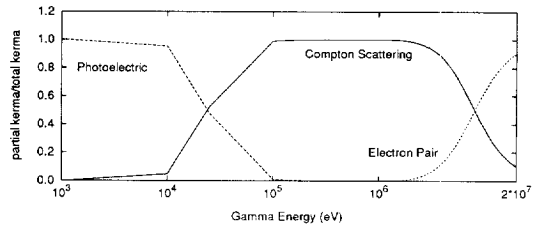

Fig. 23. Contributing gamma partial kerma factors, C.

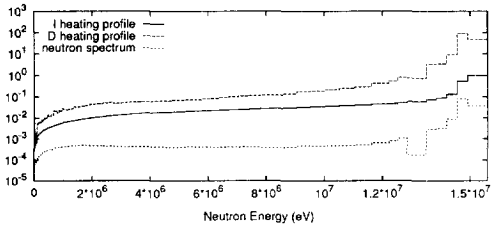

Fig. 24. Neutron profiles of Ti probe.

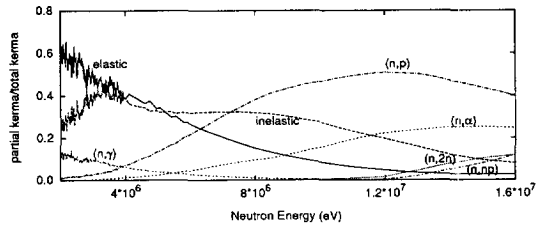

Fig. 26. Contributing neutron partial kerma factors, Ti.

were calculated and then compared and analyzed for these materials. The best kerma factor sets were selected based on physical principles, particularly energy and momentum conservation. Neutron and gamma kerma factors for individual isotopes were stored in table and graphical forms. The procedure of the analysis is summarized below.

MAZE was run first to generate pk[1-3].tape, tk[1-3].tape, gpk.tape and gtk.tape. Both partial and total kerma factors then were plotted, compared and selected. Generally speaking, when energy-angle distribution (file 6) was present and the spectrums of the recoil target and charged particles were given, the recoil result was preferred. Beside that, the balance result was usually preferred over the kinematics result because not enough data information is given for charged particle producing reactions. But the nuclear data in the basic library were far from standardized in terms of data structure and format, one really has to analyze the data on an element basis. The following examples illustrate the complexity of the analysis and the caution one has to practice when evaluating the kerma factor. Original data used in this study were taken from the FENDL [11] library.

5.1. B-11

File 6 was given for (n, 2n), inelastic to level, and charged particle producing reactions. But no energy spectrum was given for the recoil nuclides. The recoil result contained no contributions from the recoil target, and was significantly less than the balance result. Therefore, the balance result was selected.

5.2. Al-27

The gamma files for the nonelastic reaction (MT = 3) did not cover the energy range of inelastic to level reactions. Therefore, the kinematics result was selected for $E_n \leq 5.8$ MeV and the balance result was selected for $E_n \geq 5.8$ MeV.

5.3. Ti

The gamma files for the nonelastic reaction lead to negative kerma factors at the energy ranges of 1–2 and 5–11 MeV when the energy balance method was applied. Hence, the kinematics result was selected.

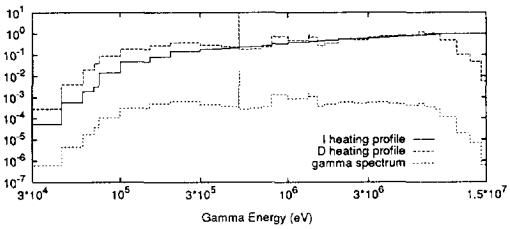

Fig. 25. Gamma profiles of Ti probe.

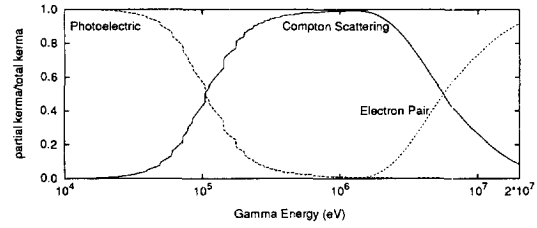

Fig. 27. Contributing gamma partial kerma factors, Ti.

Table 3
Contributions from different energy ranges, Ti

Neutron (83%)		Gamma (17%)	
Energy range (MeV)	Contribution (%)	Energy range (MeV)	Contribution (%)
0.0–0.1	~1	0.0–0.1	~3
2.1–12.5	~49	0.1–10.0	~95
12.5–15.6	~50	10.0–14.0	~2

5.4. W

The (n, 2n) and (n, 3n) reactions were very poorly described in terms of the secondary particle spectrum and gamma ray spectrum in ENDF/B-VI, leading to negative partial and total kerma factors at high energy when the balance method was applied. The kinematics result of (n, 2n) was adopted and the negative values of (n, 3n) kerma factor were set to zero.

6. The treatment of gamma production files

When gamma files are given for individual reactions the balance method can be applied to obtain partial kerma factors. In the case of a negative partial kerma factor, secondary neutron data is always kept in the evaluation. But a choice is given for the selection of partial kerma factors: either select kinematics result so that no gamma file is needed (except for (n, gamma) reaction), keep the negative partial kerma factor, or set them to be zeros.

When gamma files are given only for the (n, gamma) reaction and for the nonelastic reaction, the energy range in those files needs to be looked at. By definition, the nonelastic reaction includes the (n, gamma) reaction. But the gamma data for the nonelastic reaction usually starts at high neutron energies (100 KeV to 1 MeV range). Because the gamma contribution from the (n, gamma) reaction at low neutron energy is significant, the gamma files for both reactions are often given at the same time. MAZE checks the energy range for each reaction first, uses contribution from the (n, gamma) reaction at low energy where the nonelastic reaction files are non-existent and cuts off the (n, gamma) contribution where the two energy ranges overlap.

7. The consistency problem of nuclear data

Kerma factor evaluation has exposed a problem with the consistency of nuclear data. One obvious example of this is the negative kerma factors. Also the gamma files for nonelastic reaction often failed the energy balance check. The inconsistency of nuclear data not only affects the quality of the kerma factors, but also affects the radiation transport in terms of the production and the energy distribution of the gamma rays and the secondary neutrons, resulting in even worse heating rate estimations. Figs. 3 and 4 show the negative kerma factors generated by MAZE using the energy balance method. The sensitivity of the flux and heating rate vs. nuclear data deserves further investigations.

8. Comparison with NJOY results

8.1. Neutron kerma factor

MAZE and NJOY both adopt same calculational methods, namely, kinematics, energy balance and recoil spectra. But MAZE provides means for comparison and evaluation. The advantage is shown in the following examples. While good agreement has been achieved between MAZE and NJOY for some elements (e.g. elements of stainless steel), big differences exist for other elements (e.g. Si, B11, P). There were cases

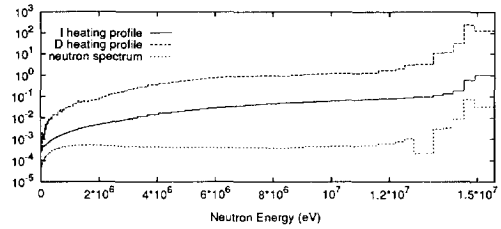

Fig. 28. Neutron profiles of Ni probe.

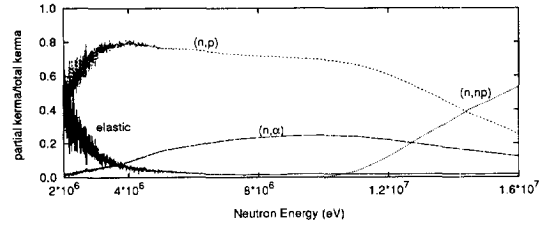

Fig. 30. Contributing neutron partial kerma factors, Ni.

where NJOY produced unreasonable results. Fig. 5 shows the partial neutron kerma factors from NJOY of the inelastic to first level reaction of Silicon. The fact that the partial kerma factors for this reaction are negative is puzzling and unreasonable, especially when it is noticed that this type of error only occurs in certain elements. Fig. 6 shows the result from MAZE for the same reaction. The difference is clearly reflected in the prompt total kerma factors shown in Fig. 7.

In the case of Boron-11, from NJOY result, the partial kerma factors of the inelastic to first level reaction are negative, shown in Fig. 8; the partial kerma factors of the (n, 2n) reaction are zero, and the partial kerma factors of (n, nα) and (n, np) are lower than the results from MAZE (Figs. 9–11). This is caused by different approaches NJOY and MAZE use to process file 6 data. For B11, file 6 was given for (n, 2n), (n, nα) and (n, np) reactions, however, no recoil spectrums were included. NJOY's approach to file 6 appeared to be to take the recoil target and the charged particle contributions. Since no recoil spectrums were given in this case, the NJOY results have only the charged particle contribution and for the (n, 2n) reaction that result is zero since no charged particle is generated from this reaction. In situations like this, MAZE has the advantage of being able to make choices among the kinematics, the balance and the recoil results which are generated at the same time. For B11, the balance result was selected in MAZE-LIB. The difference in prompt total neutron kerma factor of B11 is shown in Fig. 12.

Phosphorus gives another example of the differences between MAZE and NJOY. The neutron and gamma files are given for inelastic to continuum (MT = 91) and total inelastic (MT = 4 = 91 + 51 + ··· + 90) only. It was found that NJOY took contributions from MT = 91, instead of MT = 4 which is what MAZE took. This explains the low values of the NJOY result (see Fig. 13).

8.2. Gamma kerma factor

The three major contributing reactions for gamma kerma factors in the energy range of fusion systems are the photoelectric, Compton or incoherent scattering and pair production reactions, among which the calculation of partial kerma factor from Compton scattering reaction proves to be the most difficult. Therefore, the

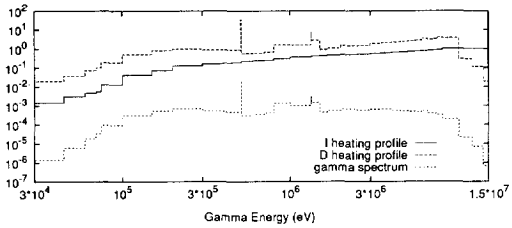

Fig. 29. Gamma profiles of Ni probe.

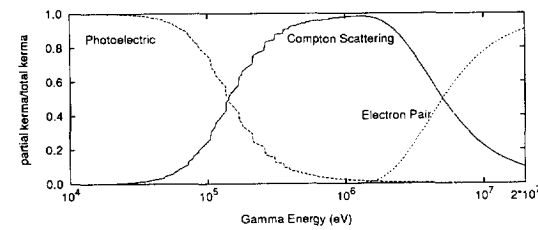

Fig. 31. Contributing gamma partial kerma factors, Ni.

Table 4
Contributions from different energy ranges, Ni

Neutron (74%)		Gamma (26%)	
Energy range (MeV)	Contribution (%)	Energy range (MeV)	Contribution (%)
0.0–3.0	~1	0.0–0.1	~2
0.3–13.5	~9	0.1–10.0	~97
13.5–15.6	~90	10.0–14.0	~1

difference between MAZE and NJOY gamma kerma factors comes mainly from the different treatment of this reaction (see Section 2.2).

Figs. 14–16 show the difference in gamma kerma factor between the MAZE and MATXS15. MATXS15 is a FENDL based library which is processed by NJOY and has a fine group structure of 175 neutron groups and 42 gamma groups. The difference is mostly reflected in the energy region where Compton scattering reaction contributes most to the total gamma kerma factors. This is made more clear from the discussions in the next chapter where the contributions from different gamma reactions to the total gamma kerma factors are given in figures. The difference between MAZE and MATXS15 seems to be less for high Z materials than for the low Z materials. The comparison of other elements shows similar trends.

9. Comparison with experiments

Since kerma factors depend on large sets of data, and complex computational algorithms, there is a strong need to verify kerma factors through comparisons with experiments. Such effort has been carried out in the present work. However, nuclear heating experiments are complex and none has ever been done with 14 MeV neutrons until recently. Over the last few years UCLA and JAERI scientists have conducted a series of nuclear heating experiments using the calorimetric technique. Fig. 17 illustrates the configuration of the experiment.

The 14 MeV D-T neutron source was generated using accelerated deuterium ions that bombarded a tritiated target. The energy deposited in the probe materials by neutrons and gamma rays induced a temperature change which was reflected in a change in the electrical resistance of the calorimeter. Highly sophisticated nano-voltmeters were used to measure the resistance change from which the temperature change was derived. A more detailed description of the experiments can be found in references [12–14].

Some analysis has been carried out during the UCLA/JAERI collaboration using different codes and libraries [12–14]. For the comparisons done in this work, one library, MATXS15, and one code, DORT, was used. MATXS15 is the FENDL based library processed by NJOY, it is

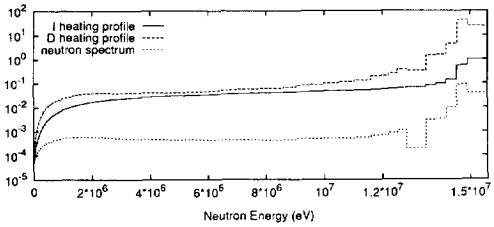

Fig. 32. Neutron profiles of Zr probe.

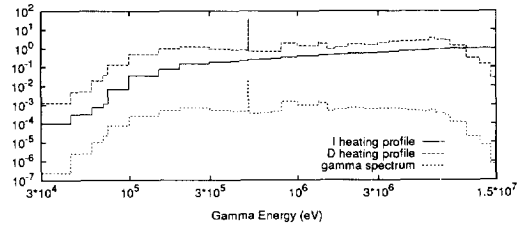

Fig. 33. Gamma profiles of Zr probe.

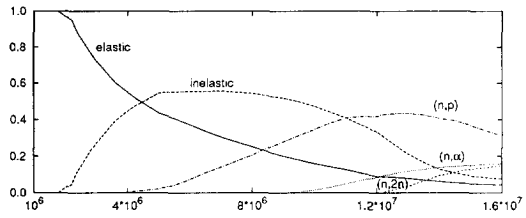

Fig. 34. Contributing neutron partial kerma factors, Zr.

also the most recent library. DORT is one of the most commonly used transport codes. This was done so that the different evaluations of the kerma factors and their effect on the calculated-to-experimental values (C/Es) could be carefully analyzed. The last series of experiments were selected for the comparison study, because of the significant improvement of the experimental technique that was developed through the UCLA/JAERI collaboration. The configuration of the experiment makes it easy to model it accurately in two dimensions.

9.1. Neutron and gamma source

The D-T neutron source was generated using accelerated deuterium ions bombarding a tritiated target. A detailed model has been established by the UCLA/JAERI scientists to simulate the D-T reaction and the neutron-target reaction to give the energy-angle distribution of the source. Figs. 18 and 19 (courtesy of Drs. Kumar and Ikeda [12–14]) show the generated source spectrum used in the neutronics calculations. Coming out of the target, the gamma to neutron ratio in intensity is about 0.18/1.

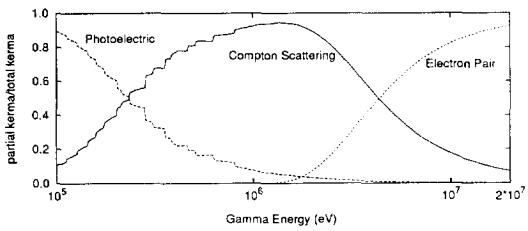

Fig. 35. Contributing gamma partial kerma factors, Zr.

9.2. Calculation vs. experiment

The UCLA/JAERI experiment was simulated in 2-D geometry using the transport code DORT and the nuclear data library MATXS15. For heating rate calculations, the kerma factors generated in this work using three approaches (kinematics, balance and recoil) were also used. The results were compared with those generated using kerma factors contained in MATXS15. Table 1 summarizes the results of the calculations. It can be seen that significant improvements in the C/Es have been achieved. The one exception was for Zirconium probe, which will be explained later. The detailed analysis of the results for each probe are given later in this section.

To analyze the calculational results in detail, the differential and integral heating profile (shown as profile D and I in the figures) are generated along with the neutron and gamma spectra for each probe. The differential file can be viewed as a sensitivity curve. It lays out the important, or sensitive, energy range for the nuclear response of interest, in this case, nuclear heating. The integral file gives the ratio of the heat deposition from energy range [0–E] to the total heat deposition

$$\left[\frac{\int_0^E K(r,E)\Phi(r,E)\mathrm{d}E}{\int_0^{E_{\max}} K(r,E)\Phi(r,E)\mathrm{d}E}\right].$$

It can be used to separate the contributing energy range from the non-contributing energy range. The contributing energy range is the energy range over which the kerma factor is really tested with the C/Es. In this set of experiment, the probe is so close to the targets, the contributing neutron energy range is centered at the peak of the neutron source spectrum around 14.1 MeV. The contributing gamma energy range is centered at a few 100 KeV. The important neutron and gamma partial kerma factors over the contributing energy range are also shown.

The magnitude of differential curve is relative and the unit is in w source^{-1} lethargy^{-1}. The unit of spectrum is in 1 source^{-1} lethargy^{-1}.

Table 5
Contributions from different energy ranges, Zr

Neutron (33%)		Gamma (67%)	
Energy range (MeV)	Contribution (%)	Energy range (MeV)	Contribution (%)
0.0–1.6	~1	0.0–0.1	~1
1.6–13.8	~9	0.1–8.0	~97
13.8–15.6	~90	8.0–14.0	~2

Given in the following are summaries of analysis for different probes.

9.2.1. Carbon probe

Neutron and gamma heating profile in the probe are given in Figs. 20 and 21. Neutron heating dominates the total heating, contributing 99% to the total heating. The neutron heating comes mainly from the energy range of 11–15 MeV and gamma heating comes mainly from the energy range of 0.1–10 MeV. Table 2 summarizes the contributions from the different energy ranges in more detail. From Figs. 22 and 23, it is evident that the partial kerma factors of elastic and inelastic scattering reactions are the two major contributors to the neutron heating and the gamma heating comes predominately from Compton scattering.

9.2.2. Titanium probe

From Figs. 24–27 and Table 3 the following observations are made. Neutron heating contributes 83% to the total heating; 14 MeV neutrons account for 50% of the neutron energy deposition and the contribution from neutrons with energy less than 2 MeV is negligible. The major contributors to the neutron heating are inelastic (n, α) and (n, p) reactions. Gamma heating comes predominately from the 0.1 to 10 MeV energy range, where Compton scattering dominates.

9.2.3. Nickel probe

The neutron heating contributes 74% to the total heating. The dominating neutron energy range is around 14 MeV where the major reactions are (n, p), (n, α) and (n, np). The gamma profile is similar to that of Titanium (see Figs. 28–31 and Table 4).

9.2.4. Zirconium probe

Neutron heating comes mainly from the inelastic (n, α) and (n, p) reactions. Here gamma heating contributes 67% to the total heating (see Figs. 32–35 and Table 5).

9.2.5. Tungsten probe

For a high Z material like tungsten, gamma heating dominates the total heating even when it is very close to the source. In this case, the gamma heating contributes 93% to the total heating. The three gamma reactions all make significant contributions, while the Compton scattering dominates around a few MeV energy range. The elastic, inelastic and (n, 2n) reactions are major contributors to the neutron heating (see Figs. 36–39 and Table 6).

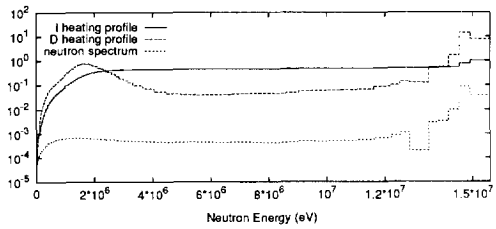

Fig. 36. Neutron profiles of W probe.

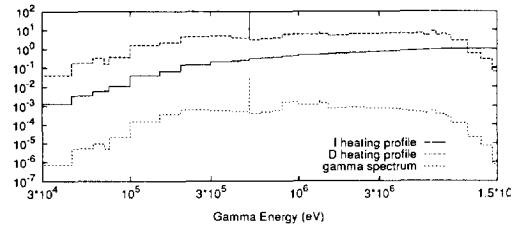

Fig. 37. Gamma profiles of W probe.

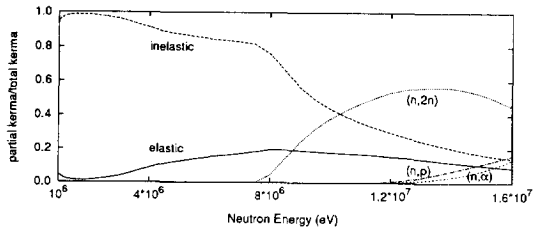

Fig. 38. Contributing neutron partial kerma factors, W.

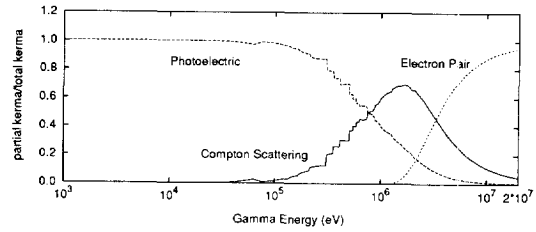

Fig. 39. Contributing gamma partial kerma factors, W.

9.2.6. Lead probe

Like tungsten, lead is a high Z material. The dominating heat source is from the gamma reactions which accounts for 92% of the total heating rate (see Figs. 40–43 and Table 7).

9.3. Source of the uncertainty

If we take the experimental error of 5–10% as reported in Ref. [14], most of the C/Es will be beyond the margins of error (>1.1 or <0.9). Since nuclear heating is calculated in the form:

$$H(\boldsymbol{r}) = \int_0^{E_{\max}} \Phi(\boldsymbol{r}, E) K(\boldsymbol{r}, E)\, \mathrm{d}E$$

the errors can be introduced either from the uncertainty in the flux ($\Phi(\boldsymbol{r}, E)$), or the uncertainty in the kerma factors ($K(\boldsymbol{r}, E)$), or both.

In this set of experiments, the error from the transport calculation has been minimized by both fixing the uncollided flux at the probe sites and the careful design of the geometric configuration of the experiment. As can be seen from Fig. 17, the probe was located very close to the source, thus an error of 1 mm in its position would lead to a 4–5% difference in the uncollided flux alone. Instead of determining it manually the position of the probe was deduced from the reaction rate ^{93}Nb(n, 2n)^{92m}Nb measured in the front and back of the probe, so that the flux of the starting group (around 14 MeV) in the neutronics transport calculation would be very close to the measurement [14]. In this way the uncertainty in the flux was minimized. This conclusion is valid since the neutron spectra in the probes were centered around the 14 MeV energy range. Therefore, it is highly suspected that the major sources of the uncertainty came from the basic nuclear data and the kerma factor calculations.

Through the kerma factor evaluation process it was found that the gamma files for certain elements contain large inconsistencies, leading to negative kerma factors or big differences between the kinematics and balance results. It is also found that different evaluations also lead to different kerma factor sets with the same basic nuclear data libraries. That is the case here with MAZE and NJOY.

Conversion factors for experimental results (raw data) can also contribute to the uncertainty in nuclear heating prediction. The experimental results used in this comparison study were given in [14] as an average temperature rise per source neutron per second along with the specific heat that is needed to convert the temperature rise into a heating rate. The conversion was carried out as:

$$\underset{\text{Measured value}}{\frac{\mathrm{K}}{\text{source s}^{-1}}} \times \underset{\text{Specific heat}}{\frac{\text{Joule}}{\text{g K}^{-1}}} \times \underset{\text{Density}}{\frac{\text{g}}{\text{cm}^3}} \times \underset{\text{Volume}}{\text{cm}^3} = \underset{\text{Calculated value}}{\frac{\text{Joule}}{\text{source s}^{-1}}}$$

Table 6
Contributions from different energy ranges, W

Neutron (7%)		Gamma (93%)	
Energy range (MeV)	Contribution (%)	Energy range (MeV)	Contribution (%)
0.0–0.3	~1	0.0–0.1	~1
0.3–13.0	~49	0.1–10.0	~92
13.0–15.6	~50	10.0–14.0	~7

The following is a probe by probe discussion of the major source of the uncertainty in the nuclear heating prediction and the explanation of the difference between the MAZE and MATXS15 results.

9.3.1. Carbon

The specific heat of carbon has large uncertainty, as shown in Table 1. It should be verified in future experiments.

9.3.2. Titanium

At the time of this analysis, the neutron kerma factors in MATXS15 are zeros, that is the reason for a C/E of only 0.45. In the MAZE library, the kinematics and balance neutron kerma factors result in different heating values. The reason is that the balance kerma factors make use of the gamma files for the nonelastic reaction, even though they lead to negative values, while the kinematics kerma factors ignore the possible gamma production in charged particle producing reactions due to a lack of data. That explains the higher C/E from the kinematics result. The two kerma factor sets are shown in Fig. 44.

9.3.3. Nickel

The difference between the MAZE and MATXS15 results is mainly from gamma heating. The gamma kerma factors coming out of NJOY are higher than that of MAZE for most of the elements in the high energy range (1 MeV). Fig. 45 displays the two kerma factor curves.

9.3.4. Zirconium

Although the MATXS15 results agree more with the experiment for this element, it is worth noting that the neutron and gamma kerma factors in MATXS15 are much higher than that of MAZE and the neutron kerma factors in MATXS15 are distorted by the strange behavior of the partial kerma factor of the inelastic to continuum reaction, as seen in Fig. 46 and its impact on prompt total neutron kerma factor is shown in Fig. 47. Fig. 48 displays the difference between MAZE and MATXS15 gamma kerma factor. The low thermal conductance of Zr probe could contribute to the low C/E of the MAZE result [14].

9.3.5. Tungsten

Gamma heating dominates the total heating even in the presence of the hardest fusion neutron

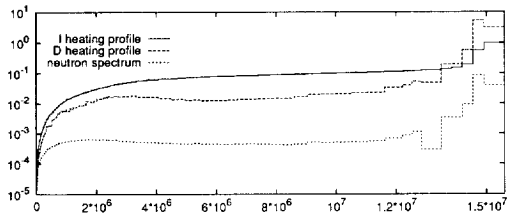

Fig. 40. Neutron profiles of Pb probe.

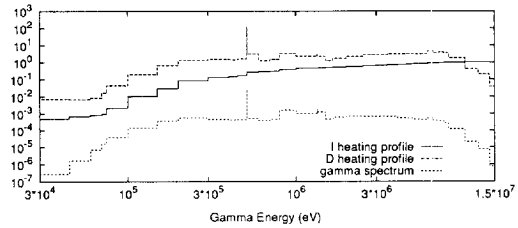

Fig. 41. Gamma profiles of Pb probe.

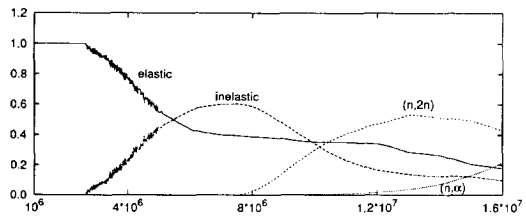

Fig. 42. Contributing neutron partial Kerma factors, Pb.

spectrum. The negative partial kerma factors of W ((n, 2n), (n, 3n)) suggest problems with the gamma production cross sections. This is evident in Fig. 49. Gamma energy, when multiplied by the yield, exceeds the energy limit set by $E_n + Q$, where Q is the mass difference from the (n, 2n) reaction. Therefore the overestimation of the gamma production leads to negative partial kerma factors. As in other cases, MATXS15 gives higher C/Es due to its higher gamma kerma factors.

9.3.6. Lead

Since gamma heating dominates the total heating, the high C/E is very likely the result of high gamma production data.

The above discussions illustrate that there are many factors affecting the C/Es. Different process codes could generate quite different response functions despite the fact that they start with the same basic nuclear data library. The structure of the nuclear data is so complex that different codes may adopt different processing strategies. While neutron flux has been fixed at the probe site to the measured value, the uncertainty in the gamma production cross section affects the transport of the gamma rays. The fact that the C/Es in most cases are much larger than 1.0, especially for the high Z material, suggest the gamma production is overestimated, although more experimental data will be needed to establish the trend. Auxiliary data such as the specific heat, which can easily vary a few percent, in the case of Carbon, the difference is as large as 24%, could also affect the nuclear heating prediction. The integral and differential heating profiles along with the contribution profile from the different nuclear reactions can be used for sensitivity analysis by the data evaluators to improve the basic nuclear data evaluation.

In this set of experiments, only high energy nuclear data were really tested. In case of deep penetration or complex configuration, uncertainty of the neutron transport will also affect the calculations and it will be even harder to separate the different factors involved in the uncertainty. Therefore it is suggested that in future experiments, both neutron and gamma flux be monitored on the test site.

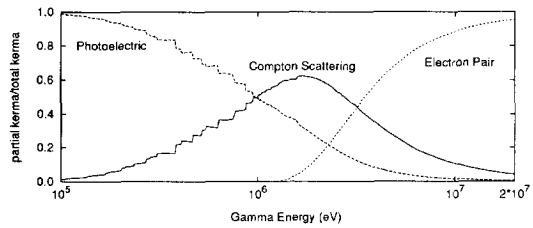

Fig. 43. Contributing gamma partial kerma factors, Pb.

10. Gamma heating in fusion reactors

Much effort has been put into neutron kerma factor evaluations. However, the gamma heating is often the most important heating source in many reactor components with heavy materials. The energy imbalance problem exposed through the neutron kerma factor analysis has a large impact on the gamma heating and was not emphasized enough in the past works. The following summaries give an overall picture of nuclear heating in a fusion reactor.

10.1. Structure material

If a steel alloy is going to be the major structure material, then gamma rays is going to be the most important heating source even in the first wall. The further back from the first wall, the more contribution from the gamma rays. This applies to other high Z materials as well.

Table 7
Contributions from different energy ranges, Pb

Neutron (4%)		Gamma (96%)	
Energy range (MeV)	Contribution (%)	Energy range (MeV)	Contribution (%)
0.0–0.3	~1	0.0–0.2	~3
0.3–13.0	~49	0.3–10.0	~96
13.0–15.6	~50	10.0–14.0	~1

10.2. Breeder

The tritium breeding reaction from Li-6 releases large amount of energy ($Q = 4.78$ MeV), usually creating a peak in the heating profile. It is worth mentioning that the uncertainty of the heating rate in solid breeder should be evaluated carefully, so the operating temperature will not go beyond the temperature window set by factors like tritium release and mechanical and chemical stability of the materials. The uncertainty in nuclear heating prediction should be taken into the consideration when selecting the solid breeder materials for the blanket.

10.3. Multiplier

The multiplier, most likely beryllium, is usually placed in front of the system, so the breeder can make the best of the extra neutrons. Therefore, neutron heating contributes the most to the total heating.

10.4. Shield

The high Z material like iron, lead and tungsten are used to stop the gamma rays and the low Z materials like B_4C are used to stop low energy neutrons. But gamma rays contribute the most to the total heating.

10.5. Magnet

Heating in the magnet system comes predominately from the gamma rays because it is positioned far behind the system. But the radiation damage to the insulator, usually copper, comes from the neutrons.

A schematic configuration of a solid breeder blanket is shown in Fig. 50, and its nuclear heating profile is shown in Fig. 51. It can be seen that the gamma heating dominates in the First Wall (FW) and the regions after the breeder (vacuum vessel, shields, and magnet). Therefore, maintaining energy balance in the neutron reaction data and generating accurate gamma production data and gamma kerma factor are very crucial in nuclear heating prediction.

11. Conclusions

A computer code, called MAZE, has been developed primarily for calculating neutron and gamma kerma factors based on an improved

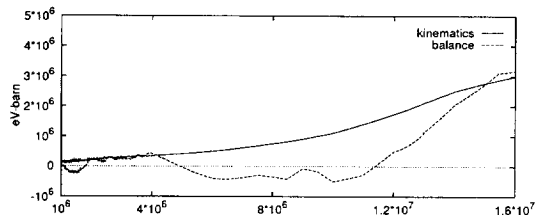

Fig. 44. Total prompt neutron kerma factor, Ti.

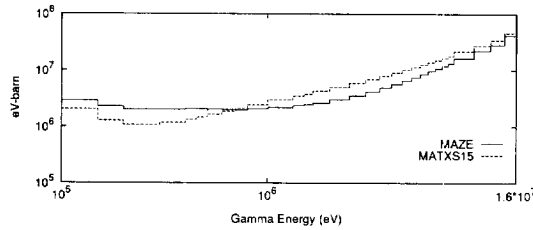

Fig. 45. Total gamma kerma factor, Ni.

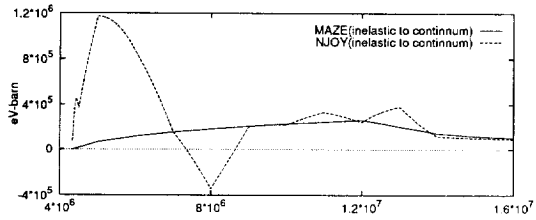

Fig. 46. Partial neutron kerma factor, Zr.

modeling and a new capability to analyze basic data and evaluate consistency in preserving energy. The code has features that allow comparison and analysis among different methods of calculating the kerma factor and it provides users with data information needed to make user-oriented selections from two to three, often different results. A kerma factor library, called MAZE-LIB, has been generated with MAZE for most of the materials of interest in fusion based on the most recent and accurate data available, FENDL library, which is the nuclear data library selected by ITER. It was shown that some data inconsistency problems in preserving the energy still exist in the FENDL library. Some problems with the widely used computer code NJOY were exposed during the process of the kerma factor evaluation carried out in this work, which is crucial at this stage of fusion research, since NJOY is the primary nuclear data processing code selected by ITER.

Comparison with nuclear heating experimental data, derived from very recent integral experiments with 14 MeV neutrons and the analysis of the uncertainty in prediction have been carried out using the newly developed kerma factors. Comparative analysis shows that the new kerma factors generated in this work result in better agreement with the experiments than those ob-

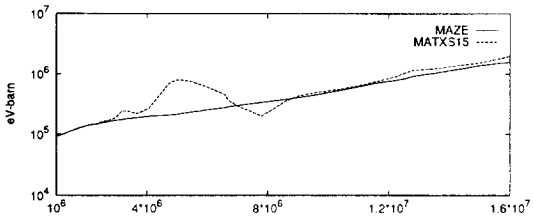

Fig. 47. Total prompt neutron kerma factor, Zr.

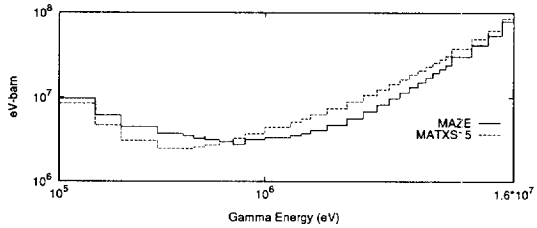

Fig. 48. Total gamma kerma factor, Zr.

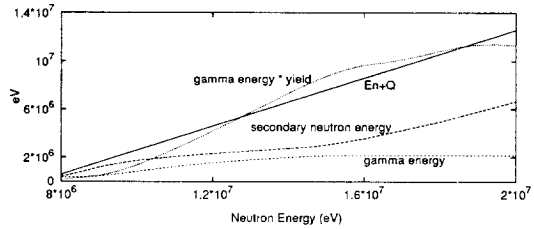

Fig. 49. Overestimation of gamma production, W184 (n, 2n) reaction.

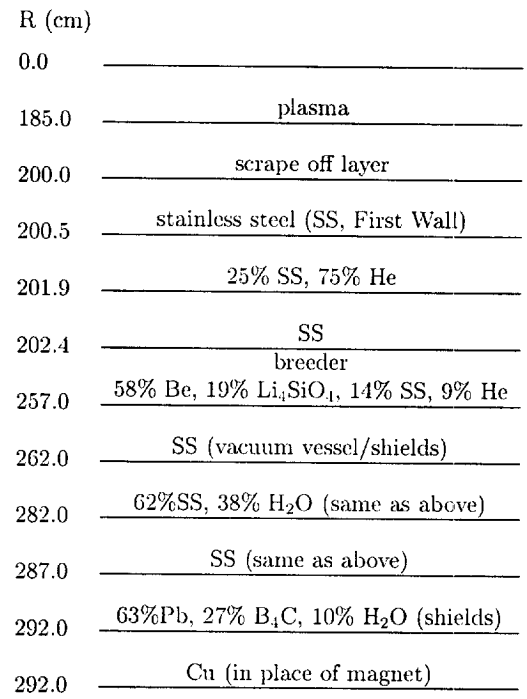

Fig. 50. Schematic of a Solid Breeder Reactor.

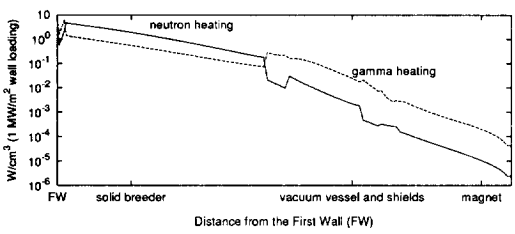

Fig. 51. Nuclear heating profile in a Solid Breeder Blanket.

tained from previous work for most of the probe materials. The C/E values obtained in this work indicate an overestimation of the gamma production in the basic nuclear data library. The integral and differential heating curves along with knowledge of the contributing reactions, which are generated in this work, could in principal provide input for sensitivity analysis and be used to improve the basic nuclear data and kerma factor evaluations.

Acknowledgements

The authors would like to acknowledge Dr Anil Kumar for his beneficial discussions and co-operation. Thanks also are due to James Eggleston for his technical assistance.

Appendix A. A material list of MAZE library

The material numbers (MAT) are adopted from the basic nuclear data library (e.g. ENDF/B, JENDL) from which the MAZE kerma factors were generated.

Material	MAT
1-H-1	125
3-Li-6	325
3-Li-7	328
4-Be-9	425
5-B-10	525
5-B-11	528
6-C-nat	600
7-N-14	710
4-N-15	720
8-O-16	825
9-F-19	925
11-Na-23	3111
12-Mg-nat	3120
13-Al-27	3131
14-Si-nat	1402
15-P-31	1525
16-S-nat	1600
17-Cl-nat	1700
19-K-nat	1900
20-Ca-nat	3200
22-Ti-nat	3220
23-V-nat	2300
24-Cr-50	2425
24-Cr-52	2431
24-Cr-53	2434
24-Cr-54	2437
25-Mn-55	2525
26-Fe-54	2625
26-Fe-56	2631
26-Fe-57	2634
26-Fe-58	2637
28-Ni-58	2825
28-Ni-60	2831
28-Ni-61	2834
28-Ni-62	2837
28-Ni-64	2843
29-Cu-63	2925
29-Cu-65	2931
40-Zr-90	4090
40-Zr-91	4091
40-Zr-92	4092
40-Zr-94	4094
40-Zr-96	4096
41-Nb-93	4193
42-Mo-nat	3420
74-W-182	7431
74-W-183	7434
74-W-184	7437
74-W-186	7443
82-Pb-206	8231
82-Pb-207	8234
82-Pb-208	8237

References

[1] M.A. Abdou and C.W. Maynard, Calculational methods for nuclear heating, Part I: Theoretical and computational algorithms, Part II: Applications to fusion reactor blankets and shields, Nucl. Sci. Eng. 56 (1975) 360–398.

[2] Y.M. Farawila, Improved Models and Results for Evaluating Neutron Kerma Factors, Ph.D. Dissertation, University of Wisconsin, 1987.

[3] P.F. Rose and C.L. Dunford (Eds.), ENDF-102, Data Formats and Procedures for the Evaluated Nuclear Data File, ENDF-6, BNL-NCS-44965, July, 1990.

[4] Anthony Foderaro, The Elements of Neutron Interaction Theory, MIT Press, Cambridge, 1971.

[5] J.H. Hubbell, Wm.J. Veigele et al., Atomic form factors, incoherent scattering functions, and photon scattering cross sections, J. Phys. Chem. Ref. Data 4 (May) (1975) 471.

[6] R. MacFarlane, NJOY 91.13, A Code System for Producing Pointwise and Multigroup Neutron and Photon Cross Sections for ENDF/B Evaluated Data, PSR-171, RSIC, 1991.

[7] M.A. Abdou, Y. Gohar and R. Wright, MACK-IV, A New Version of MACK: A Program to Calculate Nuclear Response Functions from Data in ENDF/B Format, ANL/FPP-77-5, 1978.

[8] Y.M. Farawila et al., KAOS-V Code: An Evaluation Tool for Neutron Kerma Factors and Other Nuclear Responses, ANL/FPP/TM-240, 1989.

[9] ANISN-ORNL: One-Dimensional Discrete Ordinates Transport Code System with Anisotropic Scattering, RSIC CCC-254.

[10] ONEDANT: One-Dimensional, Multigroup, Diffusion-Accelerated, Neutral-Particle Transport Code, RSIC CCC-428.

[11] S. Ganesan, Improved Evaluations and Integral Data Testing for FENDL, INDC(NDS)-312, December, 1994.

[12] A. Kumar, Y. Ikeda et al., Experimental measurements and analysis of nuclear heat deposition rates in simulated D-T neutron environment: JAERI/USDOE collaborative program on fusion neutronics experiments, Fusion Tech., 19 (May) (1991) 1979–1988.

[13] A. Kumar, Y. Ikeda et al., Direct nuclear heating measurements in fusion neutron environment and analysis, Fusion Eng. Des. 18 (1991) 397–405.

[14] Y. Ikeda, A. Kumar et al., Measurement and analysis of nuclear heat depositions in structural materials induced by D-T neutrons, Fus. Tech. 21 (1992) 2190–2196.